Acta Crystallographica Section B
Structural Science
ISSN 0108-7681

Unifying cluster-based structure models of decagonal Al–Co–Ni, Al–Co–Cu and Al–Fe–Ni

Sofia Deloudi,* Frank Fleischer and Walter Steurer

Laboratory of Crystallography, Department of Materials, ETH Zurich, Wolfgang-Pauli-Strasse 10, 8093 Zurich, Switzerland

Correspondence e-mail: deloudi@mat.ethz.ch

Received 31 May 2010
Accepted 12 October 2010

The geometrical building principles of Al-based decagonal quasicrystals and their approximants are discussed from a cluster-based approach. Our investigations cover 11 modifications with two- or four-layer periodicity in the systems Al–Co–Ni, Al–Co–Cu and Al–Fe–Ni. We identified a cluster that leads to a unifying view of all these phases. This unit cluster has ~ 20 Å diameter, four-layer periodicity along its tenfold axis and rod symmetry group $p\overline{1}02m$. The models obtained are in agreement with all the electron-density maps and electron-microscopy images available.

1. Introduction

The discovery of quasicrystals (QCs; Shechtman *et al.*, 1984) added a new dimension to our understanding of structural order. Stable QCs have been found in many binary and ternary intermetallic systems and there can no longer be any doubt about their existence as a new ordering state of matter that lacks three-dimensional periodicity (for a recent review see Steurer & Deloudi, 2008). However, despite the impressive amount of work invested in the last 25 years, laid down in more than 10 000 publications, fundamental questions still remain concerning QC growth and stability. Of course, knowledge and understanding of QC structures is an absolutely essential prerequisite to finding answers to these questions.

Our structural investigations cover a wide range of decagonal phases with two- or four-layer periodicity in the systems Al–Co–Ni (including two approximant phases), Al–Co–Cu and Al–Fe–Ni. In view of the numerous structural models already available for each phase (for a review see Steurer, 2004), we attempted to identify the general geometrical building principle(s), if any, common to all these Al-based decagonal QCs.

For our study, which was a continuation of our earlier work (Deloudi *et al.*, 2006; Deloudi & Steurer, 2007), we used the well established technique of cluster-based modeling. In this approach the structure of a decagonal phase is obtained by decoration of a particular quasiperiodic tiling with the corresponding cluster(s). We consider these clusters to be recurrent structural units rather than chemically distinct and/or mechanically stable entities (Steurer, 2006; Henley *et al.*, 2006).

Our structure models are in agreement with all the experimental data available, including electron-density maps based on X-ray diffraction (XRD), high-angle annular dark-field scanning transmission electron microscopy (HAADF-STEM, also known as the Z-contrast method) and high-resolution electron microscopy (HREM) images. Several of

Table 1
List of phases discussed in the paper.

Each one will be referred to by its phase.

Phase No.	Composition	Name	References
1	$Al_{13}Co_4$	τ^2-$Al_{13}Co_4$	Saitoh *et al.* (1999*b*); Saitoh *et al.* (1999*a*)
2	$Al_{72.5}Co_{20}Ni_{7.5}$	W–Al–Co–Ni	Sugiyama *et al.* (2002)
3	$Al_{72.5}Co_{17.5}Ni_{10}$	Basic Co-rich	Hiraga *et al.* (2002); Sugiyama *et al.* (2002)
4	$Al_{71}Co_{13}Ni_{16}$	Superstructure type I	Fleischer & Steurer (2007), *A*1
5	$Al_{70}Co_{15}Ni_{15}$	Superstructure type II	Steurer *et al.* (1993); Hiraga *et al.* (2001)
6	$Al_{69.7}Co_{10}Ni_{20.3}$	Superstructure type S1	Hiraga *et al.* (2002); Weber *et al.* (2008)
7	$Al_{72}Co_8Ni_{20}$	Basic Ni-rich	Abe & Tsai (2004)
8	$Al_{73}Fe_{22}Ni_5$/$Al_{71.6}Fe_{23.7}Ni_{4.7}$	$Al_{73}Fe_{22}Ni_5$/$Al_{71.6}Fe_{23.7}Ni_{4.7}$	Hiraga & Ohsuna (2001), *A*2
9	$Al_{70}Fe_{15}Ni_{15}$	$Al_{70}Fe_{15}Ni_{15}$	Saitoh, Tsuda, Tanaka & Tsai (1999), *A*2
10	$Al_{65}Co_{15}Cu_{20}$	$Al_{65}Co_{15}Cu_{20}$	Steurer & Kuo (1990)
11	$Al_{64}Co_{14}Cu_{22}$	$Al_{64}Co_{14}Cu_{22}$	Taniguchi & Abe (2008)

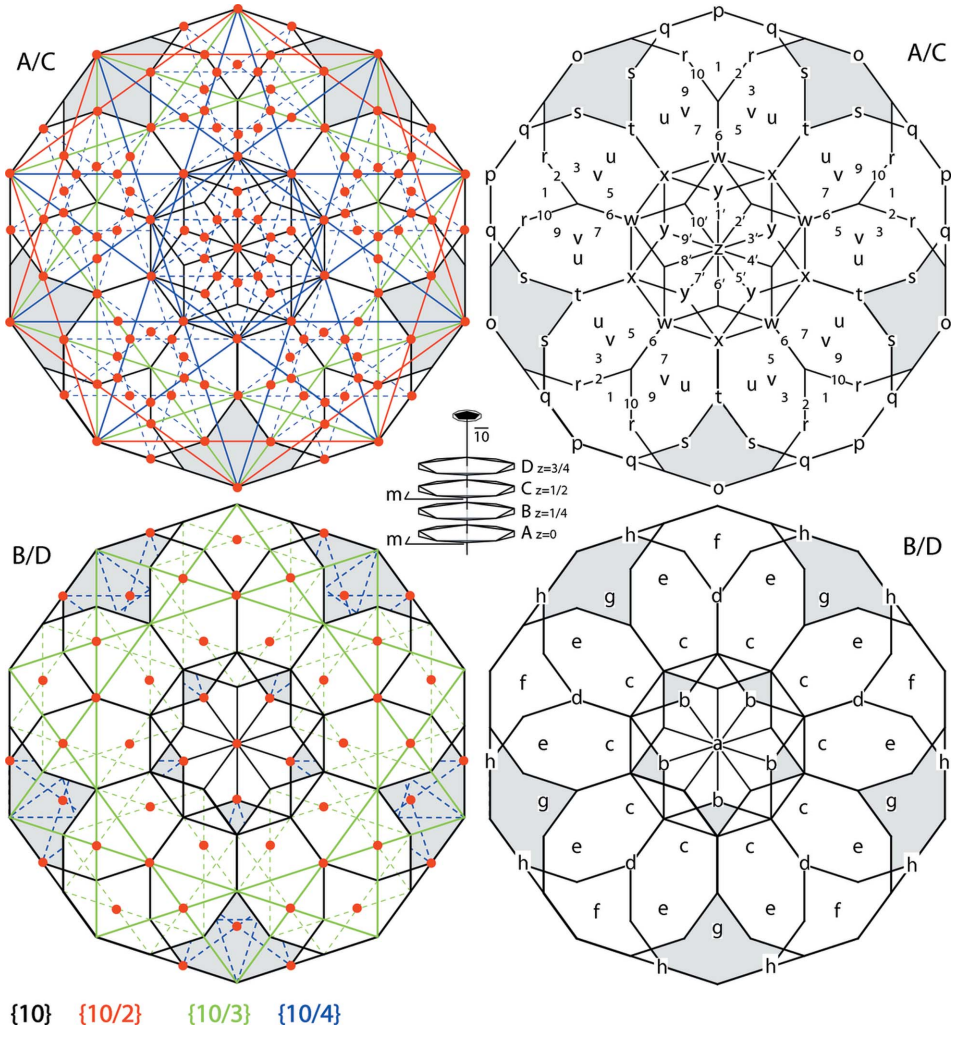

Figure 1
Idealized structure of the fundamental four-layer cluster merged to a two-layer period. Left: All ideal atomic positions can be derived as intersections of decagrams within the clusters. The Schläfli symbols of the decagrams are given on the bottom, with the corresponding color of the decagrams. Right: all atomic positions have been marked with a letter or a number. Center: layer structure of the unit cluster.

our models have already been successfully used as the basis for simulations and for direct comparison with experiments in surface structure investigations (Burkardt *et al.*, 2008, 2009; Duguet *et al.*, 2009; Mäder *et al.*, 2009; Mungan *et al.*, 2007). In this context we generated tool boxes containing three-dimensional models of all the phases investigated with up to 140.000 atoms and a diameter of ~ 800 Å.

This paper presents a universal cluster that allows unified modeling of all the investigated phases. This cluster and its geometrical properties are discussed in §2, whilst the interconnections between the phases are discussed in §3. Structural details and agreement between the models and experimental data are shown in §4.

It should be noted that the three-dimensional modeling approach used here is closely related to the five-dimensional cut-and-project approach to modeling quasiperiodic structures, while giving us some advantages. For the cut-and-project method occupation domains (hypersurfaces) are usually obtained from diffraction-data-based structure refinements, which are averaged from structural information of imperfect regions and suffer from truncation errors. Using our approach we can interpret the electron-density maps in terms of cluster-decorated tiling. By using the same clusters we can compare our result with HAADF-STEM and HREM images. Here we see the local structure of the phases and we gain information on the effect that averaging has on the structure. Additionally, we see flip positions (atomic jumps between two positions which are too near to each other to be fully occupied) that are generated by specific overlaps of clusters in the structure, and can therefore be interpreted as positions that are

favored by the competing atomic environments. This is an advantage over a purely five-dimensional cut-and-project approach, where flip positions cannot be distinguished from truncation errors affecting the borders of the occupation domains. By embedding our three-dimensional models into five-dimensional space, we can obtain occupation domains which contain more detailed information on flip positions and mixed occupation than do the occupation domains that directly result from a diffraction refinement. This will be the focus of a continuation of this work as it goes well beyond the scope of this paper.

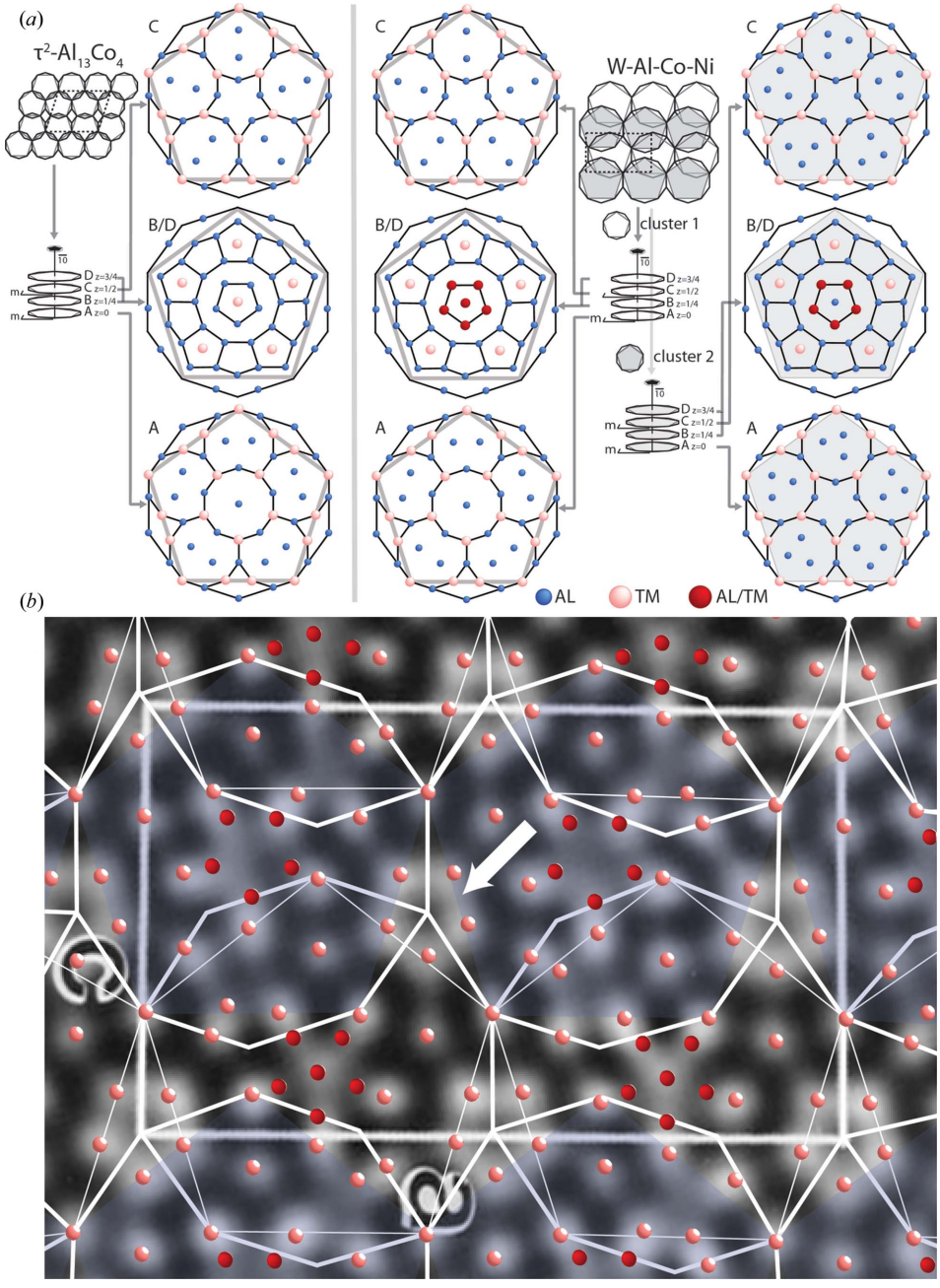

Figure 2
Phases 1 and 2 (τ^2-$Al_{13}Co_4$ and W-Al-Co-Ni): (*a*) Cluster decorated unit cell of the two approximant phases. The unit cell of phase 2 contains clusters of types 1 and 2, with a structure very similar to the structure of the decagonal phases. The atomic decoration of each layer is shown for the two phases in projection along the z direction. Clusters of types 1 and 2 have the same orientation in phase 2. (*b*) HAADF-STEM image (Hiraga *et al.*, 2002) with overlaid structural model. Only the TM sites are visible. The clusters of types 1 and 2 have similar transition metal (TM) structures and are only distinguishable by the occupied center (cluster 1) *versus* the unoccupied center (cluster 2) of the clusters. The white arrow points to a pentagonal contrast that is built by the edges of the clusters. This structural feature is predominant in all decagonal phases.

2. Unit cluster

The structures of decagonal QC can be geometrically described as periodic stackings of quasiperiodic layers or, equivalently, as two-dimensional dense packings of partially overlapping columnar clusters. The cluster centers thereby form the vertices of two-dimensional quasiperiodic tilings with decagonal diffraction symmetry (decagonal tilings, for short). Here the unit cluster is considered to be conceptually similar to the unit cell in periodic crystals. This means that the unit cluster contains all the potentially occupied sites (a kind of Wyckoff position). In the different phases different subsets are occupied. The main difference between the model and a true unit cell is that clusters can overlap in well defined ways.

Our unit cluster (~ 20 Å diameter) has a four-layer structure with a period of ~ 8 Å and rod group symmetry $p\overline{1}02m$. The layers are denoted by A ($z = 0$), B ($z \simeq 1/4$), C ($z = \frac{1}{2}$) and D ($z \simeq 3/4$), with the z coordinate along the periodic direction. Layers A and C are flat and lie in mirror planes. Layers B and D are puckered and are related to each other by the mirror planes at $z = 0$ (m_A) and $z = \frac{1}{2}$ (m_C). The structures of B and D projected along the periodic z direction are therefore not distinguishable. The differences in the structures of layers A and C are small and affect only some of the Al positions; for most of the phases the experimental resolution does not allow those positions to be identified. The two-layer cluster is merged from

four layers and describes the 4 Å average structure.

Fig. 1 (center) shows the layer structure of the four-layer unit cluster with z coordinates for each layer and symmetry elements marked. On the right and left of the figure, two different representations of the atomic decoration of merged layers A/C and B/D are given. On the left each atomic position, marked by a dot, lies on an intersection point of the lines defining a single decagram, or of intersection points of lines belonging to two decagrams. There are decagrams of two sizes in the unit cluster.

The set of large decagrams (in the Schläfli notation: one {10} decagon, two {10/2} pentagons, one {10/3} decagram, and two {10/4} pentagrams) originate from the {10} decagon forming the convex hull of the cluster. Each of $10\tau^2$ times smaller decagrams ($\tau = (1 + 5^{1/2})/2$) has one vertex in common with the convex hull of the cluster. Their centers form a decagon that is τ times smaller than the convex hull of the cluster. One additional τ^2-scaled decagram is located in the cluster center. The ten points defining the convex hull are intersection points in the {10/4} large pentagrams. On the right side of Fig. 1 all atomic positions of the unit cluster are marked by a letter or number, with symmetrically equivalent atomic positions by the same letter or number. Numbers 1–10 and 1′–10′ mark positions on partially occupied decagons.

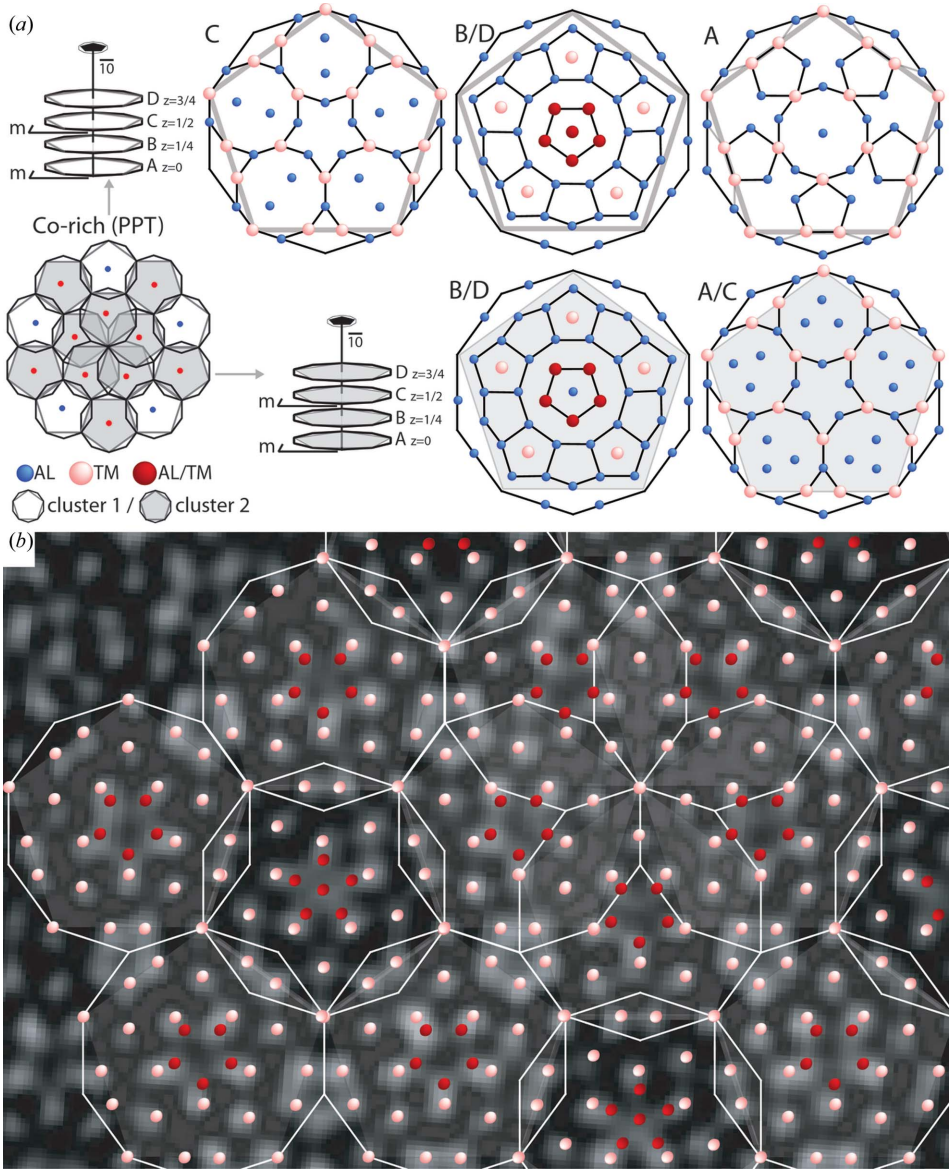

Figure 3
Phase 3 (basic Co-rich phase): (*a*) Colored pentagon tiling of type DT_1/VT_1 (Masakova *et al.*, 2005) decorated by clusters of types 1 and 2. The overlap between clusters of different type is the same as the overlap shown in Fig. 17(*b*), creating a hexagonal shaped overlap region. The atomic decoration of each layer in the two clusters is shown on the left-hand side of the figure in a projection along the periodic direction. (*b*) HAADF-STEM image (Hiraga *et al.*, 2002) with overlaid structure model (TM sites). Clusters of types 1 and 2 have similar TM substructures and are only distinguishable by the occupied center (cluster 1) *versus* the unoccupied center (cluster 2) of the clusters. We can see how the pentagonal contrast mentioned in Fig. 2 is generated by the atoms on the cluster edges. We can also see cluster 1 (center occupied by TM) in a non-overlapping configuration, where the cluster edges are visible in their unaltered form.

It should be noted that the unit cluster presented here is a new and unique cluster with geometrical properties that do not correspond to any clusters used in the literature by other authors. This type of cluster was first chosen and presented in Deloudi *et al.* (2006). The cluster that is commonly referred to as the 'standard' cluster in the literature (see Sugiyama *et al.*, 2002) has the same diameter as our cluster (∼ 20 Å), but differs by having a pentagonal ring of transition metal atoms (TMs) at the center surrounded by a decagonal ring of TMs (see white arrow in Fig. 2*b*). In our modeling approach, this distinct feature emerges at the peripheral regions of our cluster. It is generated at specific configurations of neighboring clusters that are given the underlying tiling. We have found that a gapless modeling of all phases is not possible with the 'standard cluster' or any other cluster from the literature. As an example, the standard cluster can only partially explain the Z-contrast image of the Co-rich phase shown in Fig. 3. Gaps emerge *e.g.* where one of our

Cluster 1		a	b	c	d	e	f	g	h		o	p	q	r	s	t	u	v	w	x	y	z	1'	2'	3'	4'	5'	6'	7'	8'	9'	10'
Phase 1	*B*/*D*	○	●	●	○	●	●	●	●	*A*	●	○	●		○	●			●	○		●			●						●	
										C		○	●		○	●				○	●		●					●				
Phase 2	*B*/*D*	⊙	⊙	●	○	●	●	●	●	*A*	●	○	●		○	●			●	○		●			●						●	
										C		○	●		○					○	●		●					●				
Phase 3	*B*/*D*	⊙	⊙	●	○	●	●	●	●	*A*	●	○	●		○			●	●	○		●										
										C		○	●		○					○	●		●					●				
Phase 4	*B*/*D*	○	●	●	●	○	●	●	●	*A*/*C*	●	○		●	○		$●_1$	$●_2$	●	○			●'			●'				●'		
Phase 5	*B*/*D*	○	●	●	●	○	●	●	●	*A*/*C*	●	○		●	○		$●_1$	$●_2$	●	○				●'				●'				●'
Phase 6	*B*/*D*	○	●	●	●	○	●	●	●	*A*/*C*	●	○		●	○		$●_1$	$●_2$	●	○			●'			●'				●'		
Phase 7	*B*/*D*	○	●	●	●	○	●	●	●	*A*/*C*	●	○		●	○		$●_1$	$●_2$	●	○			●'			●'				●'		
Phase 8/9	*B*/*D*	○	●	●	●	○	●	●	●	*A*/*C*	●	○		●	○		$●_1$	$●_2$	●	○					●'			●'			●'	
Phase 10	*B*/*D*	○	●	●	●	○	●	●	●	*A*/*C*	●	○		●	○		$●_1$	$●_2$	●	○					●'				●'			●'

Cluster 2		a	b	c	d	e	f	g	h		o	p	q	r	s	t	u	v	w	x	y	z	1	2	3	5	6	7	9	10
Phase 2	*B*/*D*	●	⊙	●	○	●	●	●	●	*A*	●	○	●		○	●				○	●		●			●			●	
										C	●	○	●		○	●				○	●				●			●		●	
Phase 3	*B*/*D*	●	⊙	●	○	●	●	●	●	*A*/*C*	●	○	●		○	●		●		○	●		●								
Phase 4	*B*/*D*	●	⊙	●	○	●	●	●	●	*A*/*C*		○	●		○	●		●		○	●		●								
Phase 5	*B*/*D*	●	⊙	●	○	●	●	●	●	*A*/*C*		○	●		○	●		●		○	●		●								
Phase 6	*B*/*D*	●	⊙	●	○	●	●	●	●	*A*/*C*		○	●		○	●		●		○	●		●								
Phase 7	*B*/*D*	●	⊙	●	○	●	●	●	●	*A*/*C*		○	●		⊙	●		●		○	●		●								
Phase 8/9	*B*/*D*	●	⊙	●	○	●	●	●	●	*A*/*C*		○	●		○	●		●		○	●		●								
Phase 10	*B*/*D*	●	⊙	●	○	●	●	●	●	*A*/*C*		○	●		○	●		●		○	●		●								
Phase 11	*B*/*D*	⊙	⊙	●	○	●	●	●	●	*A*/*C*	●	○	●		○	●		●		○	●		●								

Figure 4
List of site occupancies of clusters 1and 2, which are constructed by a specific decoration of the unit cluster (●Al, ○ TM, ⊙ Al/TM). Phases 1 (the τ^2-$Al_{13}Co_4$ approximant) and 11 ($Al_{64}Co_{14}Cu_{22}$) are the only single cluster phases. Phases 4–9: positions $●_1●_2$ are related Al flip positions. Occupation of the positions denoted by numbers: ● refers to 1–3, 5–7, 8–10; ●′ refers to 1′–10′.

clusters is surrounded by five others.

3. Structure models

This section provides the derivation scheme of the structure models for all the investigated phases. We will discuss the structures of 11 phases out of four systems (Al–Co, Al–Co–Ni, Al–Fe–Ni and Al–Cu–Co). The numbering of the phases follows the scheme in Table 1.

The atomic decoration of the clusters for each phase is given in Fig. 4 and will be discussed below. An overview of all the specific cluster variants can be found in Fig. 5. It should be kept in mind that our unit cluster is not equivalent to a Gummelt covering cluster (Gummelt, 2006), since it obeys different overlap rules.

3.1. Cluster 1

The atomic positions in layers *B*/*D* are identical in all phases and differ only in their chemical occupation (Fig. 4). From phase 1 to phase 2 (the two approximants τ^2-$Al_{13}Co_4$ and the W phase), mixed occupancy in the Al/TM occupation is introduced at the center of cluster 1, layer *B*/*D* (position at the center of the layer, surrounded by a small pentagon, and by TM building a larger pentagon with an *anti* orientation at the periphery of the cluster). The basic Co-rich decagonal phase (phase 3) has a cluster 1 structure very similar to that of phase 2. In particular, layers *B*/*D* and *C* in cluster 1 are identical to phase 2, as well as the TM positions in layer *A*. The positions occupied by Al in layer *A* show small differences in the peripheral regions of cluster 1.

In phase 4 (superstructure type I) the mixed Al-TM occupations are replaced with a new chemical occupation of the

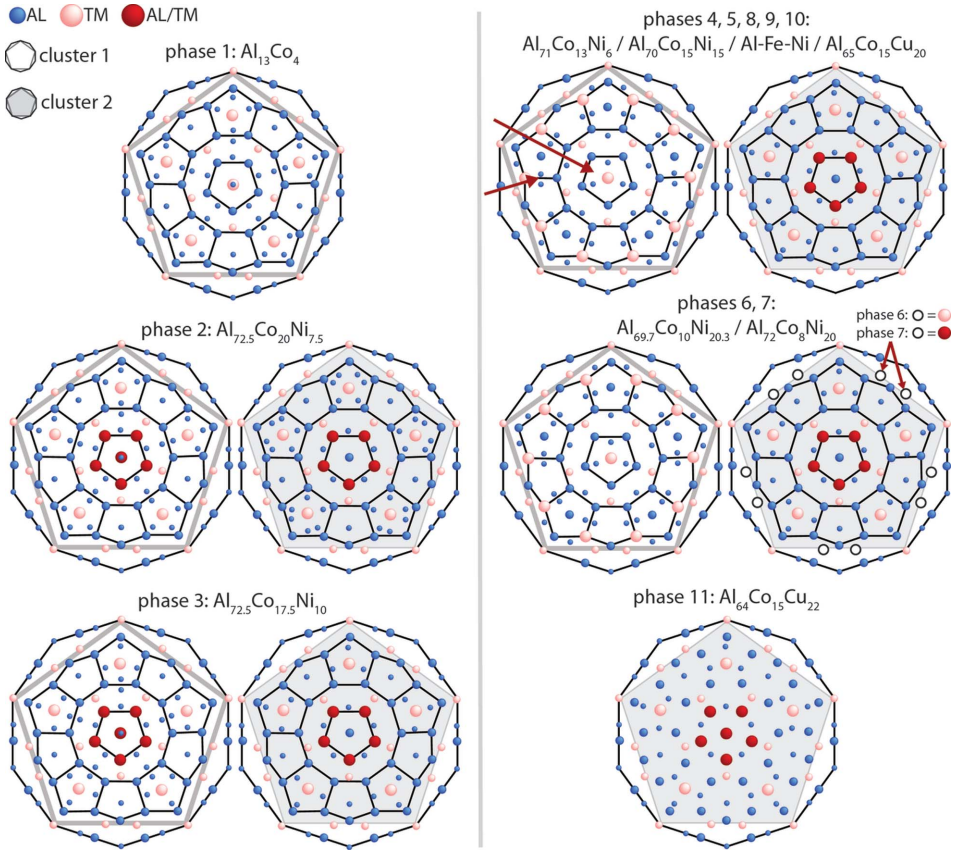

Figure 5
Clusters of all phases in projection along the periodic direction. Phases with similar clusters are shown together, arrows mark regions where the clusters differ from each other. Cluster 2 is marked by a shaded pentagon.

Phase No./name		DT_1	DT_3	DT_4	DT_5	VT_1	VT_{11}	VT_{12}	VT_{13}	Ideal tiling	Fig.
3/Basic Co-rich		•				•					3
4/Type I	*A*		*sub*				*sub*				8
	B		*sub*				*sub*				
5/Type II	*A*			•				•'			9
	B		*sub*				*sub*'				
6/S1	*A*			•				*sub*			14
	B			•				*sub*			
8/$Al_{73}Fe_{22}Ni_5$	*A*	*sub*									10
	B				*sub*						
	A'	•									10
	B'				*sub*						
9/$Al_{70}Fe_{15}Ni_{15}$		•				*sub*					16
10/$Al_{65}Co_{15}Cu_{20}$	*A*			•				*sub*'			11
	B			•				*sub*'			
11/$Al_{64}Co_{14}Cu_{22}$				•					•	•	18

Figure 6
Tilings observed in HAADF-STEM and HREM images. DT_x/VT_y refer to the Delone/Voronoi type of tilings (Masakova *et al.*, 2005). *sub*: only a subset of the expected tiles is observed; *sub*′ and •′: two additional specific coordinations of vertices (Voronoi tiles) are observed that are not allowed in ideal tiling. They are denoted 'a' and 'b' in the respective figures. *A* and *B* refer to the two observed coexisting tilings in phases 4, 5, 6, 8 and 10.

same positions in layer *B*/*D* as in phases 1–3. The TM atoms now occupy the position at the center in layer *B*/*D*, and they build a decagonal ring around the center at the periphery. Layer *A*/*C* shows the same occupation by TM atoms as layers *A* and *C* in phases 1–3 and differs in the Al occupation. In particular, we see a jump in the occupation from position q to r (from the border of the cluster to a position nearer to the center) and the introduction of systematic flip positions at u–v (building a ring of flips at the periphery of the cluster).

Phases 5–10 (superstructure type II, superstructure type S1, basic Ni-rich, $Al_{73}Fe_{22}Ni_5$, $Al_{70}Fe_{15}Ni_{15}$, $Al_{65}Co_{15}Cu_{20}$) have identical *B*/*D* layers (same as phase 4) and an almost identical *A*/*C* layer to phase 4, including TM positions and systematic flip positions for Al at u–v. They all differ in the preference of occupation of the flip positions u–v, as we will see later in detailed phase discussions. Al atoms at the periphery of the cluster in layer *A*/*C* occupy different positions in phases 5, 8, 9 and 10, while the occupation in phases 6 and 7 is identical to phase 4.

As for the most prominent similarities between clusters of type 1 in all phases we recapitulate: All TM atoms occupy the same positions (p, s and x) in layers *A*/*C* in all phases. Position q is occupied by Al in phases 1–3, which switches to position r in phases 4–10. Positions o and w are consistently occupied by Al in all phases.

Al-flip positions in layers *A*/*C* (atomic positions u and v) of phases 4–10 are denoted by $•_1$, $•_2$. There are always two kinds of occupation (different for each phase) which seem to be favored but do not occur with the same probability. In phases 4–10 three Al positions are marked with •′. This set of three positions occurs in

five different orientations in the clusters.

Layer *B*/*D* is identical in phases 4–10 and differs only in chemical occupation from phases 2–3 and 1.

3.2. Cluster 2

Layer *B*/*D* of all phases is geometrically identical to layer *B*/*D* in cluster 1 of all phases, but differs in chemical occupation (Fig. 4). Position d is occupied by TM, building a large pentagon in the periphery of the cluster as in cluster 1, phases 1–3 (τ^2-$Al_{13}Co_4$, W phase, basic Co-rich). In an *anti* orientation to this, a smaller pentagon is formed by Al/TM mixed occupation at position b around the center, as in cluster 1 of phases 2 and 3. All other positions are occupied by Al, with the exception of phase 11 ($Al_{64}Co_{14}Cu_{22}$, consisting only of type 2 clusters), where the central atom marked as position a shows additional chemical mixing Al/TM. This feature is identical to cluster 1 of phases 2 and 3.

TM atoms occupy the same positions in layer *A*/*C* in all phases. As an exception, phase 7 (basic Ni-rich) shows Al-TM mixed occupation instead of pure TM at position s. The TM positions are identical to those occupied by TM atoms in layer *A*/*C* of cluster 1 in all phases. They occupy positions p (large pentagon of TM atoms at the boundary of the cluster), s (two atoms on each line of the pentagon build by atoms at p) and x (smaller pentagon in an *anti* orientation to the large one at p).

The only difference between layer *A* and *C* of cluster 2, phase 2 (W phase) is in the positions occupied by Al at the periphery of the cluster. Those change again as we go to phase 3 (basic Co-rich). The Al occupying position o (large Al pentagon at the boundary of the cluster, in an *anti* orientation to the pentagon built by TM at position p) disappears for phases 4–10 (superstructure type I, superstructure type II, superstructure type S1, basic Ni-rich, $Al_{73}Fe_{22}Ni_5$, $Al_{70}Fe_{15}Ni_{15}$, $Al_{65}Co_{15}Cu_{20}$), and reappears for phase 11 ($Al_{64}Co_{14}Cu_{22}$). All other Al positions are identical for phases 3–11.

The clusters of type 2 are very similar in all phases. In phases 2–10 the atomic decoration of layer *B*/*D* in cluster 2 is identical. Phase 11 shows an additional Al/TM mixed occupation at the center of the layer. Layers *A*/*C* are identical for phases 4–6 and 8–10. Phase 7 shows Al/TM mixing at position s, and phases 3 and 11 have an additional Al atom occupying position o. Phase 2 is identical to phase 3 except for the Al occupation in the periphery of the cluster.

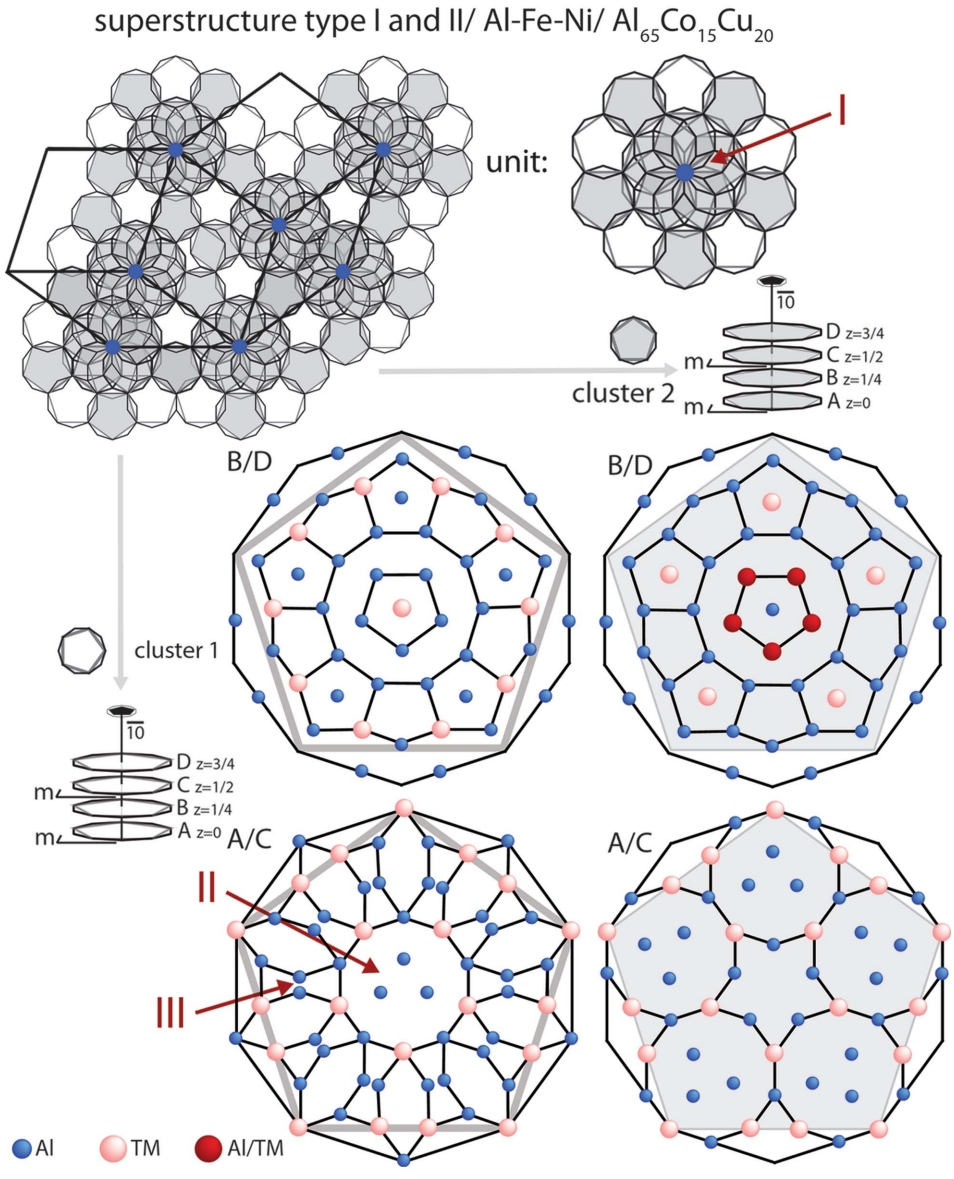

Figure 7
Phases 4, 5, 8 and 10 (superstructure types I and II, $Al_{73}Fe_{22}Ni_5$ and $Al_{65}Co_{15}Cu_{20}$): The electron-density maps of all these phases have the same underlying rhombic Penrose tiling, which is decorated by one structure motif (supercluster) consisting of 15 clusters of types 1 and 2. Depending on the decoration of the central part of the cluster (red arrow I), this supercluster can be described as either 5 clusters type 1 and 10 clusters type 2, or 10 clusters type 1 and 5 clusters type 2 (see Fig. 12). Each cluster has a layer structure consisting of layers *A*/*C* and *B*/*D*. The atomic decoration of each layer is shown in a projection along the periodic direction. The atomic decoration at the center of layer *A*/*C*, cluster 1 (red arrow II), is shown here for phase 4. Phases 5, 8 and 10 all have a group of three Al atoms in the same region, but with different occupied positions (see Figs. 4, 8, 9, 10 and 11). These three atoms break the fivefold symmetry of the cluster and occur in five different orientations. In layer *A*/*C*, cluster 1, all phases show Al-flip positions (red arrow III). The occupation probability for these flip positions differs for each phase.

In Fig. 5 we give an overview of the cluster variants of all phases. While cluster 2 does not exhibit significant differences, cluster 1 shows two distinct forms for phases 1–3 and phases 4–10. The clusters for phases 4, 5, 8, 9 and 10 are shown together, as well as the clusters for phases 6 and 7. Red arrows denote the regions where the clusters differ in their detailed structure (mainly occupation of flip positions, or chemical occupation) – see Fig. 4.

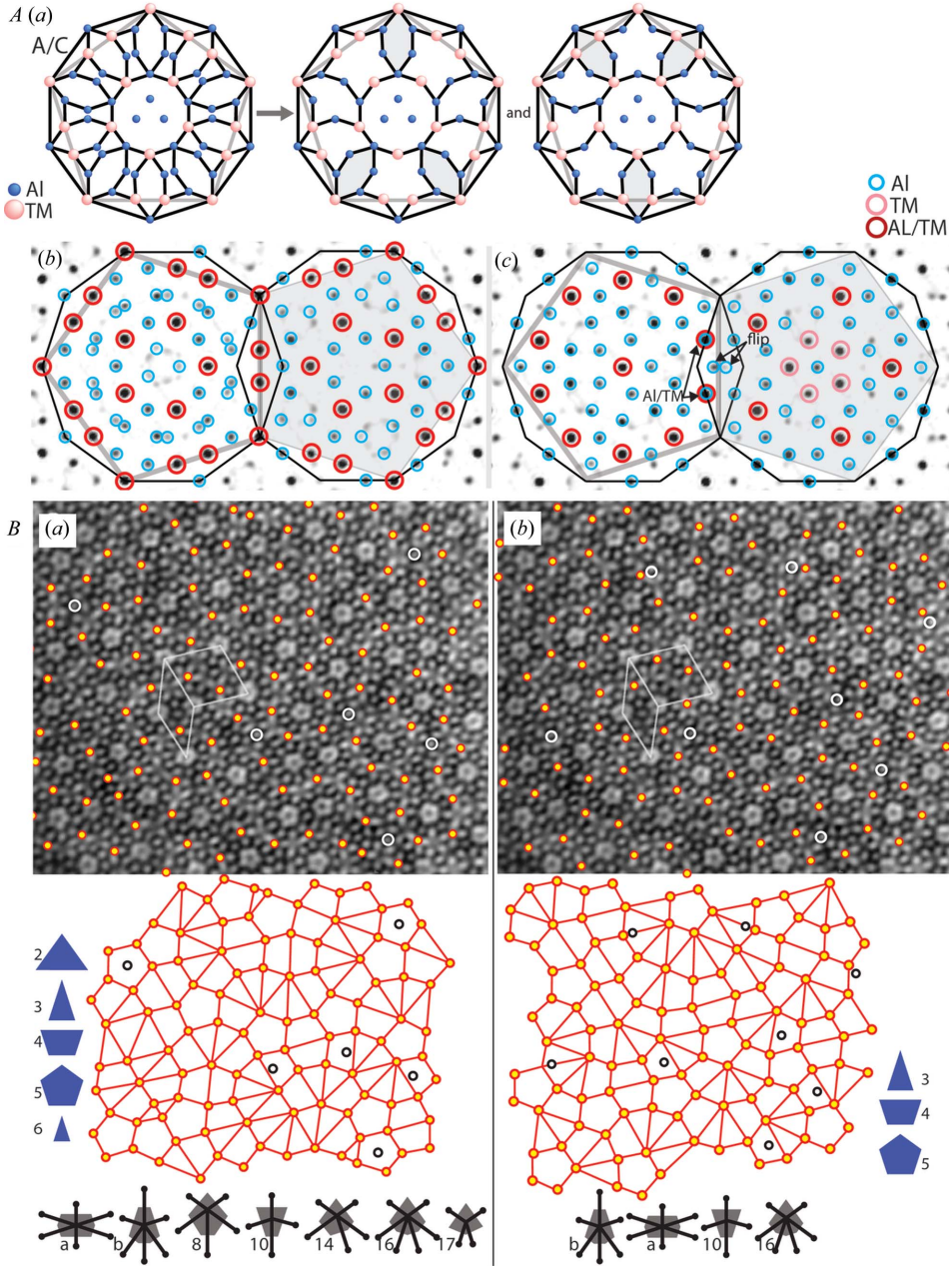

Figure 8
Phase 4 (superstructure type I): *A* (*a*) Structures of the two preferred configurations of occupied flip positions in cluster 1, layer *A*/*C* and their averaged structure. *A* (*b*) Projected electron-density map obtained from single-crystal XRD (see *A*1) with overlaid cluster types 1 and 2, layer *A*/*C*. Cluster 1 is shown with the average occupation of flip positions and one orientation. *A* (*c*) Projected electron-density map with overlaid cluster types 1 and 2, layer *B*/*D*. *B*: One and the same HAADF-STEM image (Hiraga *et al.*, 2002) is shown in *B* (*a*) and *B* (*b*). There are two types of tilings needed, both non-ideal pentagon tilings of type VT_{12}/DT_4 (Masakova *et al.*, 2005), whose vertices give the cluster centers. In *B* (*a*) and *B* (*b*) we see the positions of cluster types 1/2 marked with black/red circles. All clusters have the same orientation within one image and an *anti* orientation between images.

3.3. Tilings

As shown in the previous sections, the ideal structures of the clusters needed to build the structures of the 11 distinct phases are remarkably similar. Indeed, the largest differences in the structures result from the tilings that we need in order to construct the models and to explain the observed data. The choice of different tilings, even if they were decorated with identical clusters, can lead to varying local atomic environments resulting from overlapping regions of the clusters. Furthermore, a specific overlap of clusters can form in the overlapping regions of clusters of similar type. Those generated clusters contribute to the overall stability of the structure by forming further global tilings themselves (subtilings), and therefore by enhancing the configurational entropy of the structure.

One problem in defining the underlying tilings of the structures lies in the versatility of the structure itself. When is a cluster an essential generating cluster and when is it a result of overlapping between clusters? How do we minimize subjective bias when identifying cluster centers?

We have obtained the tilings presented in this work by applying the following directives. We define cluster centers only where needed to obtain the complete structure without gaps or contradictions to the data. If by that choice further clusters are generated within the structure, we view them as secondary clusters. Generally, this is unambiguous as the optimal choice reduces the number of parameters in our model (secondary clusters do not generate the observed structure without gaps; optimal cluster choices lead to more regular tilings and simpler models without the loss of accuracy; the generation of secondary clusters follows rules that can be consistently observed throughout the structure). Finally, the most important directive in our modeling is consistency. This means that if a choice of models is still ambiguous within the accuracy of the data, the best model is the

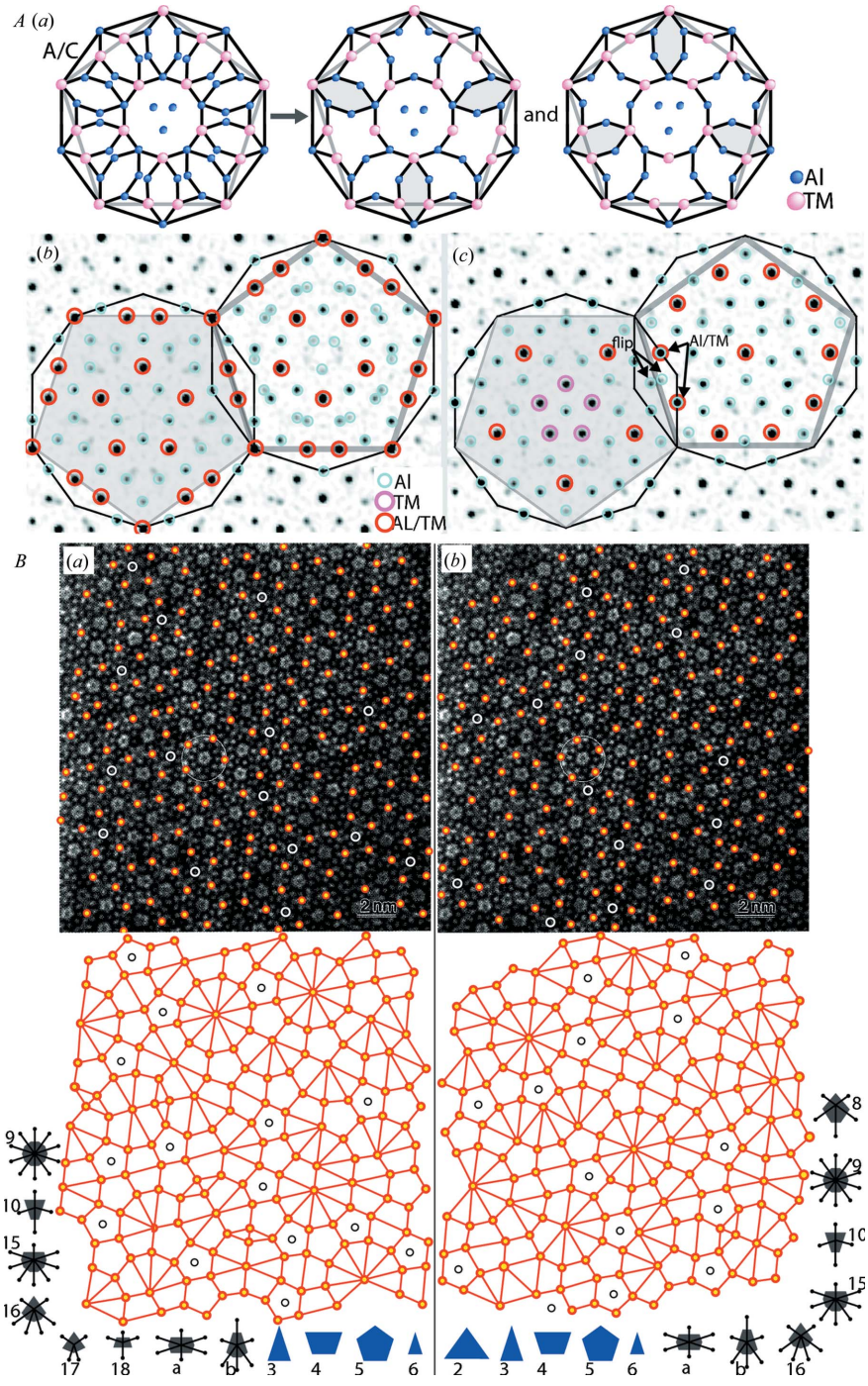

Figure 9
Phase 5 (superstructure type II): *A* (*a*) Structures of the two preferred configurations of occupied flip positions in cluster 1, layer *A*/*C* and their averaged structure. *A* (*b*) Projected electron-density map obtained from single-crystal XRD (refinement structure of the decagonal $Al_{70}Co_{15}Cu_{15}$ phase; Steurer *et al.*, 1993) with overlaid cluster types 1 and 2, layer *A*/*C*. Cluster 1 is shown with averaged occupation of flip positions and one orientation. *A* (*c*) Projected electron-density map with overlaid clusters types 1 and 2, layer *B*/*D*. *B*: One and the same HAADF-STEM image (Hiraga *et al.*, 2001) is shown in (*a*) and (*b*). There are two types of tilings needed, both non-ideal pentagon tilings of type VT_{12}/DT_4 (Masakova *et al.*, 2005), whose vertices give the centers of the clusters. In *B* (*a*) and *B* (*b*) we see the positions of cluster types 1/2 marked with white/red circles. All clusters have the same orientation within one image, and an *anti* orientation between images. In the lower part of the figure we see the extracted tilings. (*a*) and (*b*) Cluster type 1 occupies all pentagons of one orientation (*anti* orientation of clusters and occupied pentagons in *a* and *b*) and builds a subtiling, contrary to phase 4 which does not show this degree of order.

one that shows consistency within the modeled phase, as well as to the models obtained for all the related phases.

The next section discusses each model in detail and its agreement with experiment. The essence of modeling regarding the underlying tilings can be summarized as follows.

(i) The globally averaged structures, which can be obtained from single-crystal XRD, and the local structures (averaged over the sample thickness) observed by HAADF-STEM or HREM, show the same basic clusters but different underlying tilings. This means that the local tiling may differ considerably from the globally quasiperiodically averaged one.

(ii) Observed flip positions in electron-density maps can be related to overlapping clusters.

(iii) The white arrow in Fig. 2(*b*) marks a characteristic pentagonal contrast resulting from pairs of atoms located close to the cluster boundary. This feature is predominant in all the decagonal phases studied and is always formed by the cluster boundaries. The unit cluster itself does not contain this structural feature since then it would not allow a gapless modeling of all phases. In some cases clusters with this pentagonal feature at the center ('standard cluster') have been used (Sugiyama *et al.*, 2002). The resulting tilings in this work are therefore different from those found in the literature, where the standard cluster has been used. However, their relation to each other is well defined, since the standard cluster is generated and contained in our structure models.

(iv) In the structure of the periodic approximant phase 2 (W–Al–Co–Ni), neighboring clusters of the same type have one edge in common and show a shift of $z = \frac{1}{2}$ to each other. Therefore, each layer of the unit cell perpendicular to the z direction (periodic direction) contains layers *A* and *C* of each cluster type, or layers *B* and *D*, respectively. We suspect that such shifts are also present in the decagonal phases but not modeled in this work. They would not lead to different underlying tilings, but to a coloring of the tilings according to the shifts. With future 8 Å structure refinements, it would be possible to model the coloring of the underlying tilings as well.

Regarding the nature of the underlying tilings for the HAADF-STEM and HREM images, we can make the following comments.

The tilings obtained from HAADF-STEM and HREM images are pentagon tilings of different types. They are given for each phase in Fig. 6 with a reference to the corresponding figures. Only phase 11 ($Al_{64}Co_{14}Cu_{22}$) shows a patch of ideal quasiperiodic tiling. It can be constructed from one cluster of type 2 in one orientation. This is the only cluster which needs generating.

Phases 3, 8 and 9 (basic Co-rich phase and the two phases in the system Al–Fe–Ni) need two clusters (type 1 and 2). In phase 3 the two clusters decorate a DT_1/VT_1 (Delone/Voronoi type) tiling (Masakova *et al.*, 2005). However, we can see from HAADF-STEM images that the decorated tiling is not ideal but includes patches of periodic tile arrangements. In phase 8 ($Al_{73}Fe_{22}Ni_5$) clusters of type 2 decorate a DT_1 tiling which shows only a subset of the expected VT_1 Voronoi tiles. Clusters of type 1 decorate the centers of the large pentagonal Delone tiles.

Phases 4, 5, 6, 8 and 10 (type I, type II, S1 and $Al_{65}Co_{15}Cu_{20}$) show two coexisting pentagon tilings which are decorated by clusters of type 2. Within each of the two coexisting tilings, all clusters (type 2) have the same orientation. The clusters belonging to different tilings are in an *anti* orientation to each other. These two tilings are not generating and secondary tilings. All clusters here are generating clusters and therefore the two tilings are needed to build the structure. The result of this feature is a switching in the orientation of the predominant pentagonal shape mentioned before (white arrow in Fig. 2*b*). Its orientation depends on which of the two coexisting tilings the pentagonal shape originates from. The occurrence of the two orientations can form superstructures with two-color tilings (for the resulting tilings see the references given for the HAADF-STEM images for each phase). Symmetry breaking in the pentagonal shape can also be observed in regions where none of the two underlying tilings dominate. This will be discussed in detail in the next section. Clusters of type 1 result from certain configurations of clusters of type 2, in their overlapping regions.

The two coexisting tilings in phase 5 (type II) are of different types. They each show (as in phase 10, $Al_{65}Co_{15}Cu_{20}$) two additional identical Voronoi tiles which are forbidden in the ideal pentagon Penrose tiling (PPT). Phase 8 ($Al_{73}Fe_{22}Ni_5$) also shows two coexisting tilings consisting of cluster 1 as well as two coexisting tilings decorated by clusters of type 2.

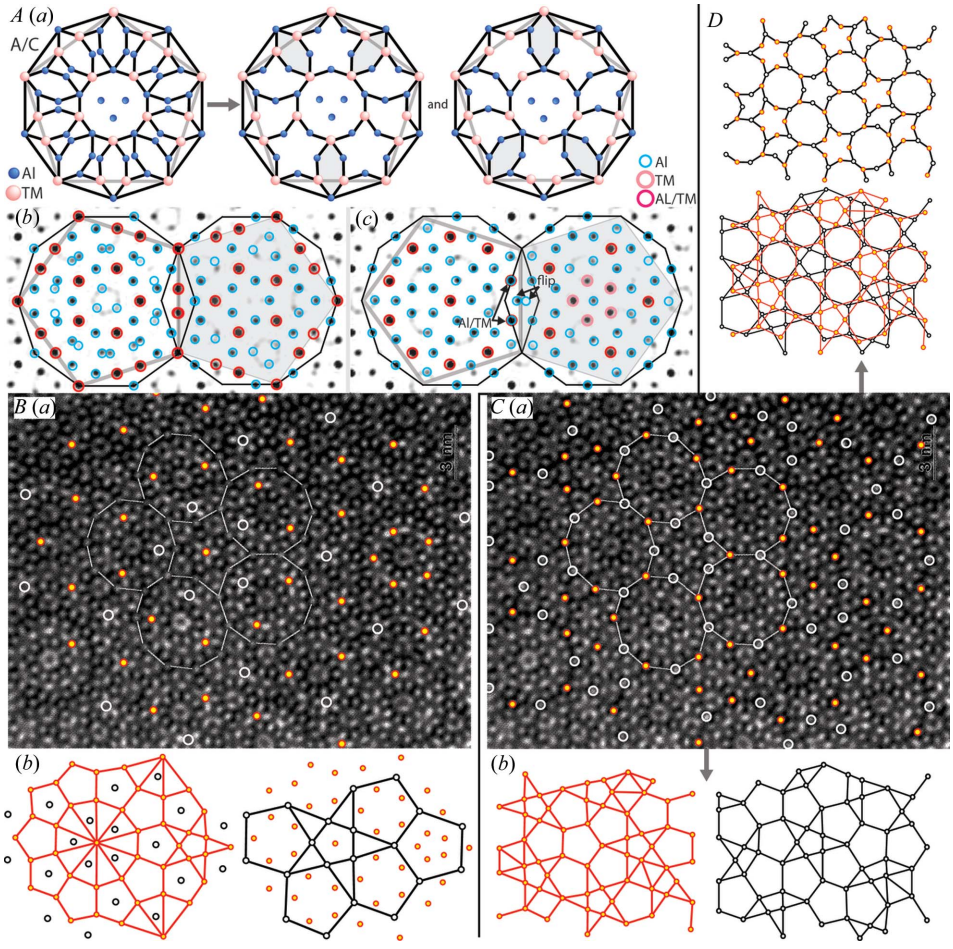

Figure 10
Phase 8 ($Al_{73}Fe_{22}Ni_5$): *A* (*a*) Structures of the two preferred configurations of occupied flip positions in cluster 1, layer *A*/*C* and their averaged structure. *A* (*b*) Projected electron-density map obtained from single-crystal XRD with overlaid cluster types 1 and 2, layer *A*/*C*. Cluster 1 is shown with an average occupation of flip positions and one orientation. *A* (*c*) Projected electron-density map with overlaid cluster types 1 and 2, layer *B*/*D*. At the edges of the clusters, we can see how overlaps can create flip positions and mixed occupancy in the structure. *B* (*a*) and *C* (*a*) the same HAADF-STEM image (Hiraga & Ohsuna, 2001) is shown. In *B* (*a*) clusters of type 2 are marked with white and red circles, distinguishing between the two possible orientations. Similarly, clusters of type 1 are marked in *C* (*a*) with white and red circles. *B* (*b*) All cluster centers (type 2) are shown on the left and on the right, as well as the two tilings built by clusters of the same orientation. *Black*: subset of DT_1, *red*: subset of DT_5 (Masakova *et al.*, 2005). *C* (*b*) Two tilings are built by clusters of type 1, each containing only clusters of the same orientation. *Red*: DT_1, *black*: subset of DT_5. *D*: From the top: tiling built by clusters of type 1 and alternating orientations; it can also be interpreted as two tilings, each containing only clusters of the same orientation [see *C* (*b*)].

4. Agreement with experiment

In this section we will discuss the models in detail and show their agreement with experiment.

4.1. Phases 1 and 2 (τ^2-$Al_{13}Co_4$ and W–Al–Co–Ni), Fig. 2

The atomic decoration of the clusters is shown for two approximants as well as an HAADF-STEM image of phase 2 (Hiraga *et al.*, 2002) with an overlaid structural model. The pentagonal contrast that is characteristic of the HAADF-STEM images of all the investigated phases is marked here by an arrow. We can see that it is generated by atoms that belong to the cluster boundaries. The amount of TM in Al/TM mixed positions ranges from 10 to 95%. This is the only phase where we have quantitative data on mixing from the XRD structure refinement. Therefore, we can say little about the expected values of the occupation factors for the mixed position. The models for all phases are purely qualitative.

4.2. Phase 3 (basic Co-rich phase), Fig. 3

Besides the atomic decoration of the clusters, an HAADF-STEM image (Hiraga *et al.*, 2002) is shown with an overlaid structure model. The underlying tiling is a pentagon tiling of the type DT_1/VT_1 (Masakova *et al.*, 2005), decorated by clusters of type 1 and 2. Only one orientation is allowed for clusters of the same type, while clusters of different types are in an *anti* orientation. In phase 2 (W phase) all clusters have the same orientation. Phase 3 shows additional overlaps of clusters of the same type, while the overlap between clusters of different type is the same as in phase 2.

In this example it is shown how different overlap rules can result in periodic or quasiperiodic arrangements of clusters. In addition to the characteristic pentagonal contrasts generated by atoms near the cluster boundaries, we can also see cluster 1 (center occupied by TM) in a non-overlapping configuration, where the cluster edges are visible in their original form. The atomic structure of such a region cannot be modeled with a cluster that contains the pentagonal contrast in its center [as is the case for the 'standard cluster' (Sugiyama *et al.*, 2002) commonly used in the literature].

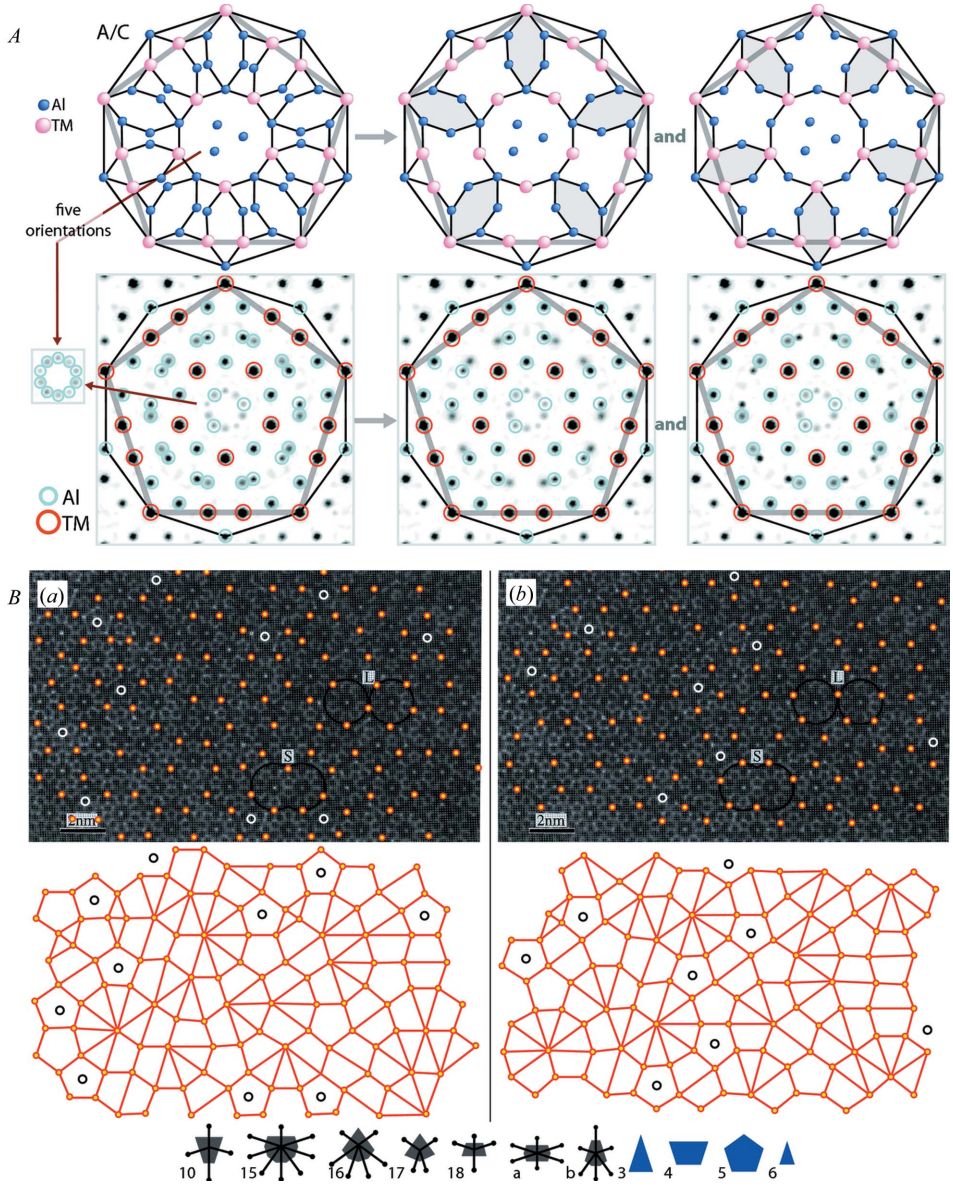

Figure 11
Phase 10 ($Al_{65}Co_{15}Cu_{20}$): *A* In the upper part of *A* the two preferred occupations of flip positions are shown (*cf.* Figs. 4 and 7). The group of three atoms in the cluster center can occur in five orientations, breaking fivefold symmetry in three cases. The two configurations maintaining fivefold symmetry seem to be favorable and occur with different probabilities. In the lower part of *A* we see the projected electron-density map (Steurer & Kuo, 1990) with overlaid cluster structures of the two preferred configurations and the averaged structure. *B*: The same HREM image (Saitoh *et al.*, 1996) is shown in *B* (*a*) and *B* (*b*). There are two types of tilings needed, both non-ideal pentagon tilings of type VT_{12}/DT_4 (Masakova *et al.*, 2005), whose vertices correspond to the cluster centers. In *B* (*a*) and *B* (*b*) we see the positions of cluster types 1/2 marked with white/red circles. All clusters have the same orientation within one image and an *anti* orientation between images.

4.3. Phases 4, 5, 8 and 10 (superstructure type I and II, $Al_{73}Fe_{22}Ni_5$ and $Al_{65}Co_{15}Cu_{20}$), Fig. 7

A patch of tiling underlying the electron-density maps obtained from single-crystal XRD is shown with the decorating supercluster, as well as the atomic decoration of clusters 1 and 2. The globally averaged XRD-based structures are very similar for phases 4, 5, 8 and 10, while their local structures obtained from HAADF-STEM images show larger differences (*cf.*

here with Figs. 8, 9, 10 and 11). The cluster structures differ only in the occupation of specific flip positions, which can also lead to symmetry breaking of the ideal cluster.

4.4. Phase 4 (superstructure type I), Fig. 8

Fig. 8 shows the structures of the two preferred configurations of the occupied flip positions in cluster 1, layer *A*/*C*, and their averaged structure, the projected electron-density map obtained from single-crystal XRD (see *Appendix A*1) with overlaid clusters type 1 and 2, layer *A*/*C*, an HAADF-STEM image (Hiraga *et al.*, 2002) with two types of underlying tilings (the same image is shown twice), and the extracted tilings with their Delone and Voronoi tiles.

4.5. Phase 5 (superstructure type II), Fig. 9

The figure shows the structures of the two preferred configurations of occupied flip positions in cluster 1, layer *A*/*C*, and their averaged structure, the projected electron-density map obtained from single-crystal XRD (refinement structure of the decagonal $Al_{70}Co_{15}Cu_{15}$ phase; Steurer *et al.*, 1993) with overlaid cluster types 1 and 2, layer *A*/*C*, an HAADF-STEM image (Hiraga *et al.*, 2001) with two types of underlying tilings (the same image is shown two times), as well as the extracted tilings with their Delone and Voronoi tiles. Clusters of type 1 result in overlap regions from clusters of type 2, within pentagons of one orientation in the tilings. They build a subtiling, as opposed to phase 4 (superstructure type I) which does not show this degree of order.

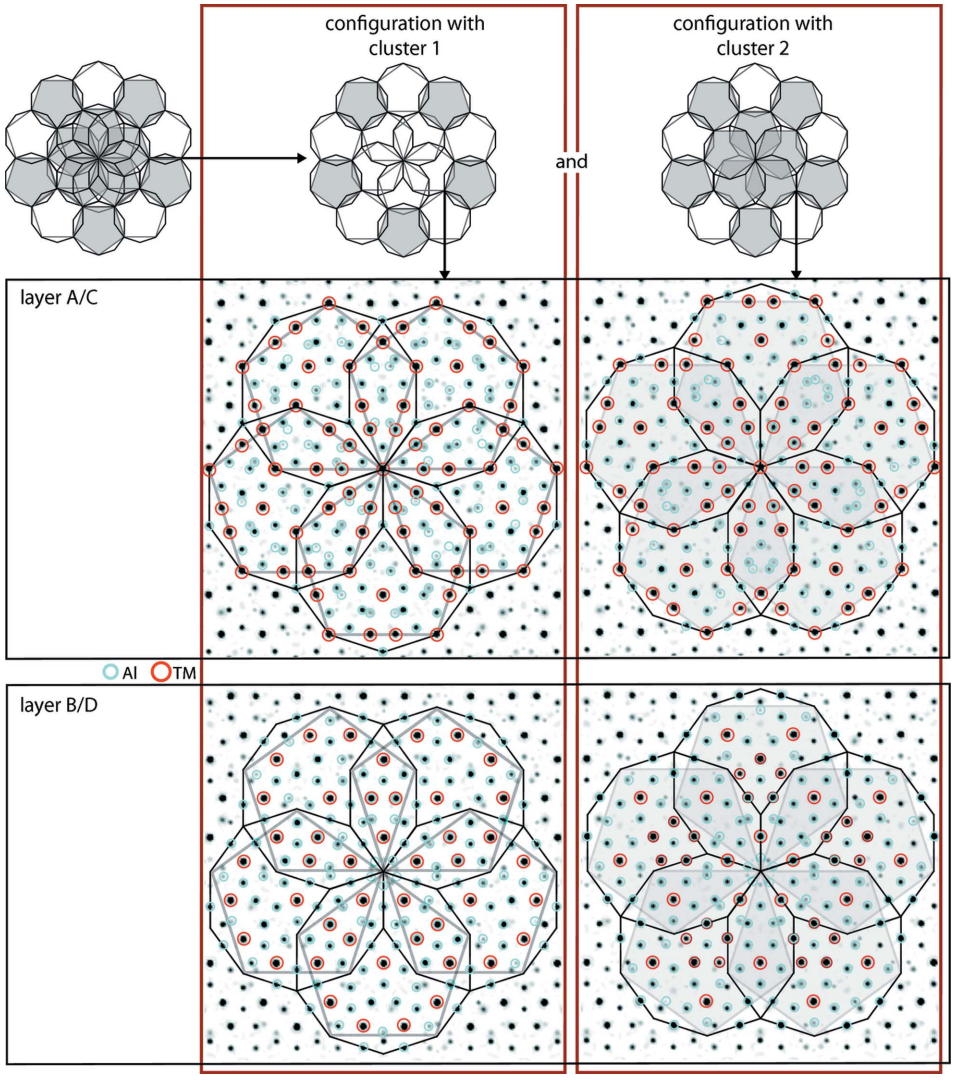

Figure 12
Phase 10 ($Al_{65}Co_{15}Cu_{20}$): Projected electron-density map obtained from single-crystal XRD (Steurer & Kuo, 1990) with overlaid structures of the two preferred configurations at the center of the superclusters. One consists of five clusters of type 1, the other of five clusters of type 2. When two clusters overlap, most atomic positions of each of the two contributing clusters do match, as we will see later. If two atomic positions do not coincide, they generate flip positions. The two resulting atomic structures are realised in the decagonal phases.

4.6. Phase 8 ($Al_{73}Fe_{22}Ni_5$), Fig. 10

In this figure the two preferred occupations of the flip positions in cluster 1, layer *A*/*C*, are depicted. Furthermore, the projected electron-density map obtained from single-crystal XRD with an overlaid structure model, an HAADF-STEM image (Hiraga & Ohsuna, 2001) with overlaid tiling vertices corresponding to cluster centers, as well as the extracted tilings are shown. The preferred occupation of the flip positions and the three atoms in the cluster center break the fivefold symmetry of the unit cluster. The averaged cluster, however, shows fivefold symmetry since all clusters occur in five orientations in the structure. An example of how overlaps can introduce flip positions and mixed occupancy can be seen at the edges of the clusters.

The HAADF-STEM image (Hiraga & Ohsuna, 2001) shows several underlying tilings. For clusters of type 2 we have two intertwined pentagon tilings, each one decorated with clusters of the same orientation. Clusters of type 1 can decorate a decagon-boat-star tiling with alternating orientation of clusters at neighboring vertices, or two intertwined pentagon tilings with clusters of only one orientation each.

4.7. Phase 10 ($Al_{65}Co_{15}Cu_{20}$), Figs. 11 and 12

In Fig. 11 the two preferred occupations of flip positions are depicted, as is an XRD-based electron density map (Steurer & Kuo, 1990) with overlaid structure model, an HREM image (Saitoh *et al.*, 1996) with two types of underlying tilings (the same image is shown two times) as well as the extracted tilings with their Delone and Voronoi tiles.

Both underlying tilings shown here (occupied with clusters of type 2) are needed. They are occupied by clusters of the same type but different orientations, and they coexist in the structure. In certain regions the atoms near the cluster boundaries form an atomic configuration that can be seen as a pentagonal contrast in the HREM and HAADF-STEM images of all phases (see arrow in Fig. 3). Depending on which cluster boundaries generate this pentagonal contrast, the orientation of the pentagon can change. If the contributing clusters do not all have the same orientation, then the symmetry of the pentagonal shape will be broken. Changing orientations of the pentagons or symmetry breaking in this region is an important feature of several phases [see Figs. 10 (orientation of the pentagons is not clearly visible here), 8, 9 and 14].

Clusters of type 1 result in overlap regions from clusters of type 2 within pentagons of one orientation in the tilings. The center of the supercluster depicted in Fig. 7 shows two different configurations, consisting of five clusters of type 1 or of five clusters of type 2. Both configurations are compared with an XRD-based electron-density map (Steurer & Kuo, 1990) in Fig. 12, using phase 10 ($Al_{65}Co_{15}Cu_{20}$) as an example. All atomic positions generated by the two configurations coincide with the electron density obtained from the XRD data. This means that the two resulting atomic structures are realised in the decagonal phases, since they can be observed in the averaged structure.

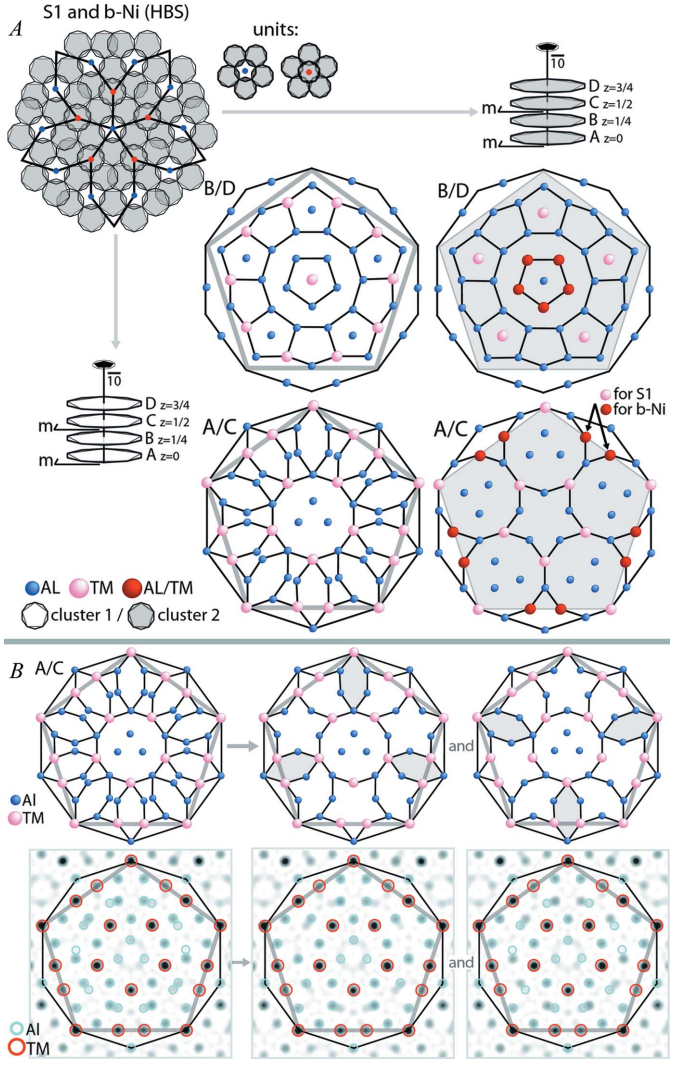

Figure 13
Phases 6 and 7 (S1 and basic Ni-rich phase): *A* Hexagon-boat-star (HBS) tiling decorated by two structural motifs, each one consisting of six clusters of type 1 and 2. The atomic decoration of each cluster layer is shown in a projection along the periodic direction. Arrows mark the positions where the chemical occupations of the ideal averaged structures of phases 6 and 7 differ. Phase 7 (S1): *B* Projected electron-density map obtained from single-crystal XRD (decagonal $Al_{69.7}Co_{10}Ni_{20.3}$; Weber *et al.*, 2008) with overlaid structures of the two preferred configurations at the center of the superclusters.

4.8. Phases 6 and 7 (S1 and basic Ni-rich phase), Fig. 13

The underlying tiling of XRD-based electron-density maps, the two structural motifs that decorate the tiling and the

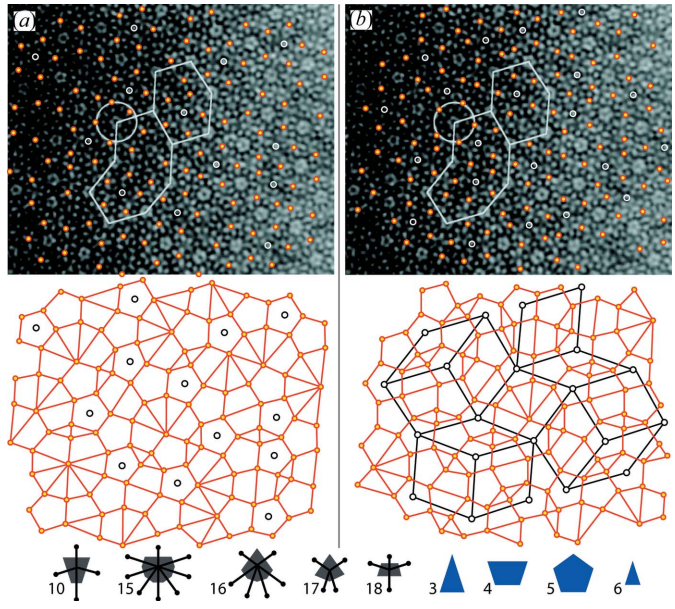

Figure 14
Phase 6 (S1): The same HAADF-STEM image (Hiraga *et al.*, 2002) is shown in (*a*) and (*b*). There are two types of tilings, both non-ideal pentagon tilings of type VT_{12}/DT_4 (Masakova *et al.*, 2005), whose vertices correspond to the cluster centers. In (*a*) and (*b*) the positions of cluster types 1/2 are marked with white/red circles. All clusters have the same orientation within one image and an *anti* orientation between images. In the lower part, the extracted tilings are depicted. As in phase 5 (type II), cluster type 1 occupies in (*a*) and (*b*) all pentagons of one orientation (*anti* orientation in *a* and *b*) and builds a subtiling. The Delone and Voronoi tiles at the bottom of the figure are the same for the two tilings built by cluster 2.

atomic structure of the clusters are shown. The two cluster types appear in the two orientations. Differences in the chemical occupation of the clusters between phases 6 and 7 can also lead to a different occupation of flip positions within the same layer.

4.9. Phase 6 (S1), Fig. 14

One and the same HAADF-STEM image (Hiraga *et al.*, 2002) is depicted with two types of underlying tilings as well as the extracted tilings with their Delone and Voronoi tiles. As in phase 5 (type II), cluster type 1 occupies in (*a*) and (*b*) all pentagons of one orientation (*anti*-orientation in *a* and *b*) and builds a subtiling.

4.10. Phase 7 (basic Ni-rich phase), Fig. 15

In this figure we see a HAADF-STEM image (Abe & Tsai, 2004), where the TM sites of clusters of type 1 and 2 are visible, with an overlaid structure model as well as an extracted part of the HAADF-STEM image, where the next adjoining cluster is placed subsequently in (*b*)–(*d*), leading to changes in the chemical occupation in the structure.

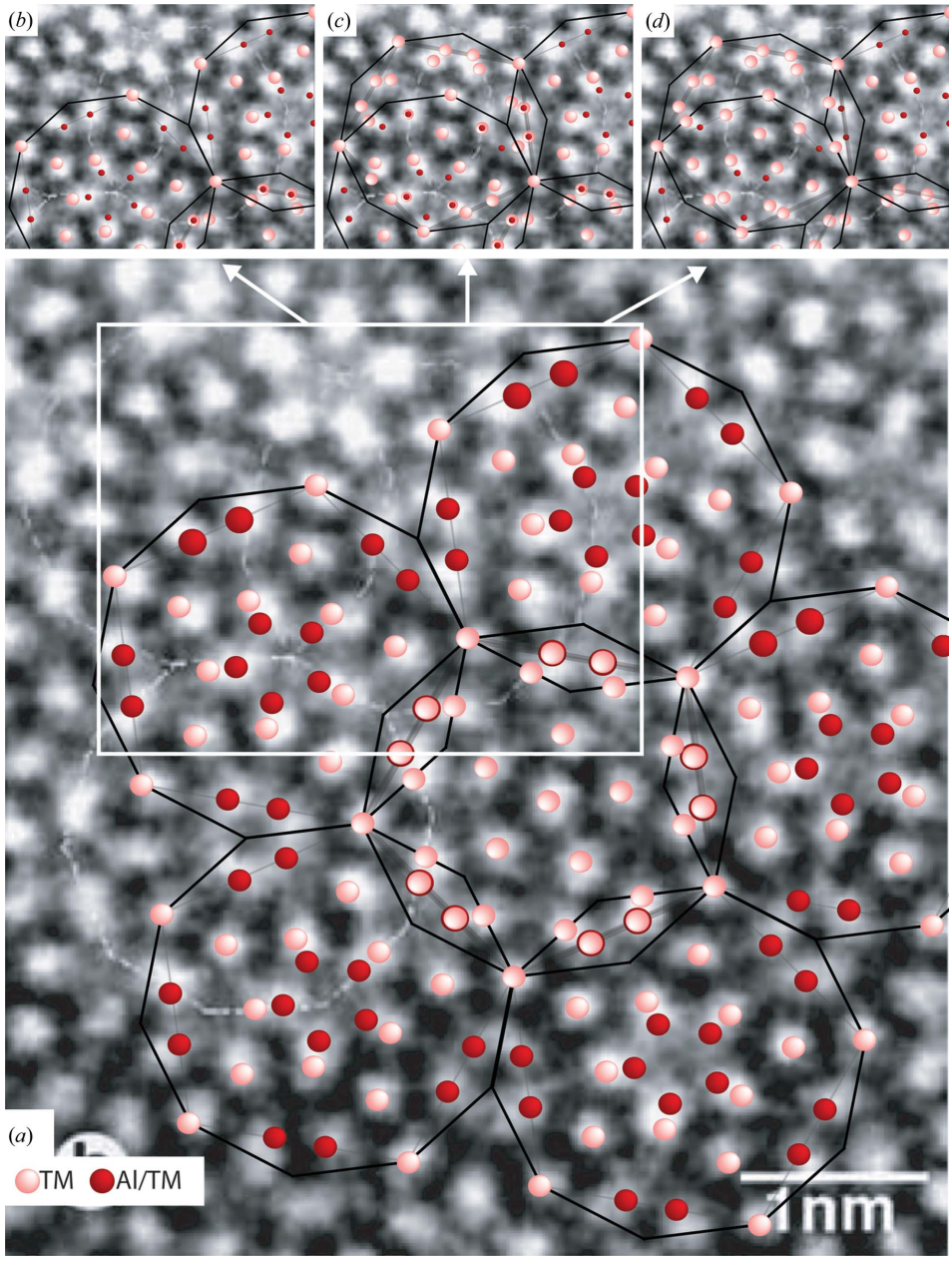

Figure 15
Phase 7 (basic Ni-rich phase) HAADF-STEM image (Abe & Tsai, 2004) with clusters of types 1 and 2, and TM as well as Al/TM sites marked. The structure shows a part that also corresponds to one of the building units of the averaged structure (see Fig. 11*a*). On the upper part, we show a smaller part of the HAADF-STEM image, where the next adjoining cluster is placed subsequently in (*b*)–(*d*), leading to changes in the chemical occupation in the structure.

4.11. Phase 9 ($Al_{70}Fe_{15}Ni_{15}$), Fig. 16

The figure shows a HAADF-STEM image (Saitoh *et al.*, 1999*a*) with overlaid tiling vertices corresponding to cluster centers, the extracted tiling with drawn-in Delone and Voronoi tiles and the boundaries of the clusters that decorate the tiling. The vertices of the underlying tiling give the centers of clusters of type 2 with one orientation. The centers of the large pentagons in the tiling are again decorated by clusters of type 2 (in an *anti* orientation to the tiling clusters) and clusters of type 1, depending on the orientation of the pentagons. These clusters do not result in overlaps of clusters on the main tiling, but are needed to generate the structure model. In Fig. 16(*c*) the similarity of the resulting structure to the averaged structure observed in the electron-density maps is obvious (*cf.* Fig. 7).

4.12. Phase 11 ($Al_{64}Co_{14}Cu_{22}$), Figs. 17 and 18

Here we show the atomic decoration of the cluster and of overlap regions, a HAADF-STEM image (Taniguchi & Abe, 2008) with and without an overlaid structure model as well as an HAADF-STEM image (Taniguchi & Abe, 2008) with overlaid tiling vertices corresponding to cluster centers. The high-resolution image in Fig. 15 even allows verification of

Al sites of the model. The HAADF-STEM image in Fig. 16 allows the identification of a large section of the underlying tiling, a pentagon tiling of type VT_{13}/DT_5 (Masakova *et al.*, 2005), with all expected Delone and Voronoi tiles. In order to model the structure, only one cluster (type 2) in one orientation is needed. However, clusters of type 1 can be observed (*generated* clusters) as they result from specific overlaps of clusters of type 2 (*generating* clusters).

5. Concluding remarks

In this study we have demonstrated that our definition of a fundamental unit cluster allows a systematic description of all structurally known two- and four-layer Al-based decagonal quasicrystals including approximant phases. All the models obtained are in excellent agreement with the available high-resolution experimental data. This modeling approach also allows a geometric interpretation of the observed positions in the investigated phases as equally favorable positions in the overlapping cluster regions. The observed cluster overlaps can be interpreted as clusters partially containing the neighboring clusters, offering an ansatz for the development of a corresponding growth model. The change from the formation of approximants to the formation of quasicrystals is particularly interesting regarding the differences of the observed overlap rules between clusters. In this context, further studies should focus on the correlations of composition and mixed occupancy with the observed overlap rules. Since Al and TM, as well as Co and Ni have different preferred atomic environments, we expect the observed overlap rules to correlate directly with allowed flexibility in the chemical occupation and with the occupation of flip positions. The observed geometry corresponds only to an averaged structure solution (for XRD data averaged over the five-dimensional unit cell and for HAADF-STEM and HREM images over the thickness of the sample) and must vary as the composition changes. We expect Ni to show a high degree of mixing with Co, and therefore to introduce a gradual change in the preferred atomic environments of mixed occupancy positions as more and more Ni is introduced in the structure.

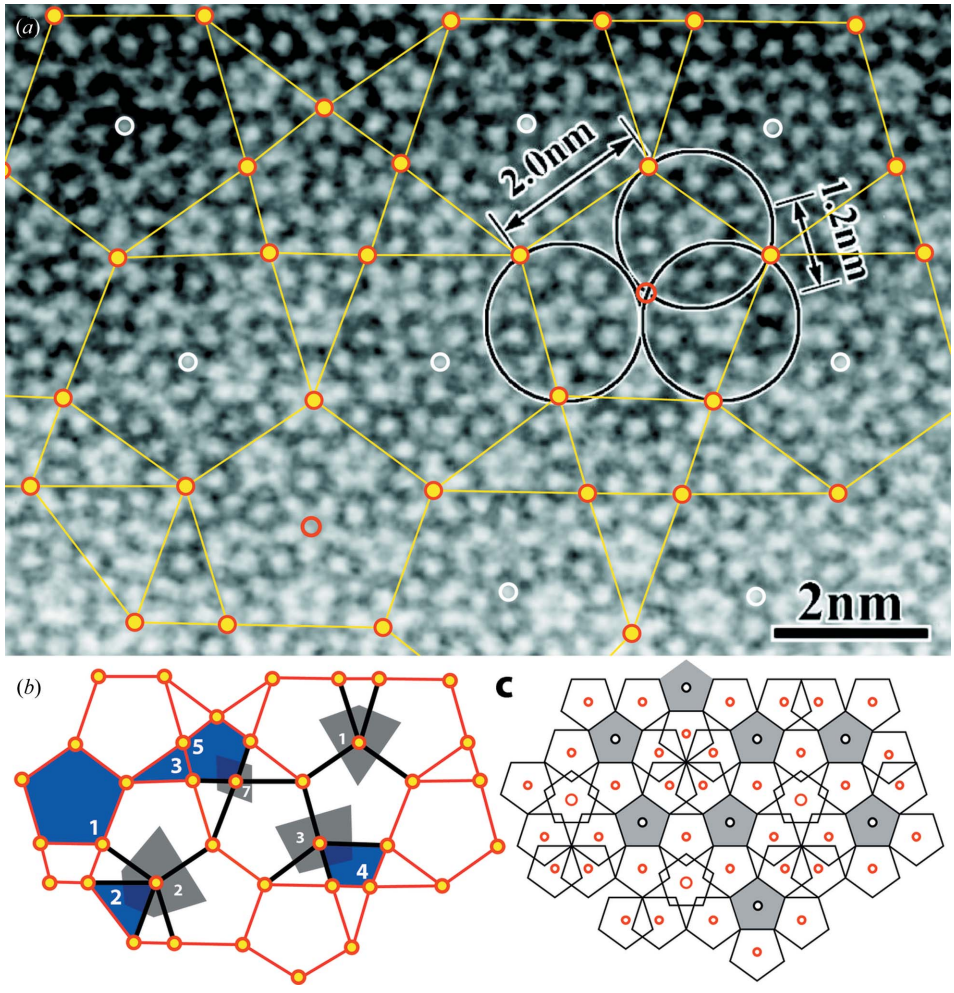

Figure 16
Phase 9 ($Al_{70}Fe_{15}Ni_{15}$): (*a*) HAADF-STEM image (Saitoh *et al.*, 1999*a*) with overlaid tiling vertices corresponding to cluster centers; clusters of type 1 are marked by white circles and have one orientation. There are two orientations for clusters of type 2, marked by yellow filled and empty red circles. Clusters of type 1 (white circles) are in an *anti* orientation to the clusters of type 2 at the tiling vertices (red circles with yellow filling). (*b*) The extracted tiling, a non-ideal pentagon tiling of type VT_1/DT_1 (Masakova *et al.*, 2005), and its Delone (blue) and Voronoi (gray) tiles. All Delone tiles, but only a subset of the expected Voronoi tiles are observed. (*c*) Outlines of the clusters decorating the tiling.

APPENDIX *A*

For two phases additional structural information was needed and single-crystal XRD studies were performed. The experimental details are described in the following.

A1. Phase 4, Superstructure type (I)

A sample of ~ 1 g with initial composition $Al_{71}Co_{13}Ni_{16}$ was pre-alloyed using an electric arc furnace. The as-cast sample was kept in corundum crucibles and sealed in evacuated and Ar-filled (400 mbar) silica glass ampoules before a subsequent annealing procedure in a calibrated temperature-controlled furnace. According to the phase diagram

and the stability region of the type I phase, the following heat treatment was applied: the sample was first heated to 1350 K and slowly cooled to the first annealing temperature. Then it was stepwise annealed at 1220 K for 120 h, at 1100 K for 150 h and in a last treatment at 1000 K for 150 h. The cooling rate between these single steps was 1 K h^{-1}. Finally, the sample was water quenched. The chemical composition of the grown crystals was determined to $Al_{70.6\,(3)}Co_{13.3\,(3)}Ni_{16.1(2)}$ by microprobe analysis, based on 32 single point measurements. Backscattered electron images confirmed the sample to be single phase.

A single-crystal XRD data set was collected at the Swiss–Norwegian beamline (SNBL) at the European Synchrotron Radiation Facility (ESRF), Grenoble, France, using an imaging-plate detector system. Two data sets were collected with different exposure times; one data set with short exposure time to prevent saturation of the strong reflections, and one data set with a longer exposure time in order to optimize the counting statistics of weak reflections.

The decagonal phase was identified as a type I structure. The type I structure, a fivefold superstructure of the basic structure, contains satellite reflections. For the present study, only main reflections were used for the structure solution, which was performed within the five-dimensional approach using the charge-flipping algorithm (Oszlányi & Sütő, 2004; Palatinus, 2004). The charge-flipping calculations were run without any symmetry constraint in the space group $P1$. The data set consists of 19 785 observed reflections. Additional low-density elimination iterations were performed to reduce the noise in the electron-density maps. 100 successful runs were averaged in order to generate high-quality electron-density maps (Fleischer *et al.*, 2010).

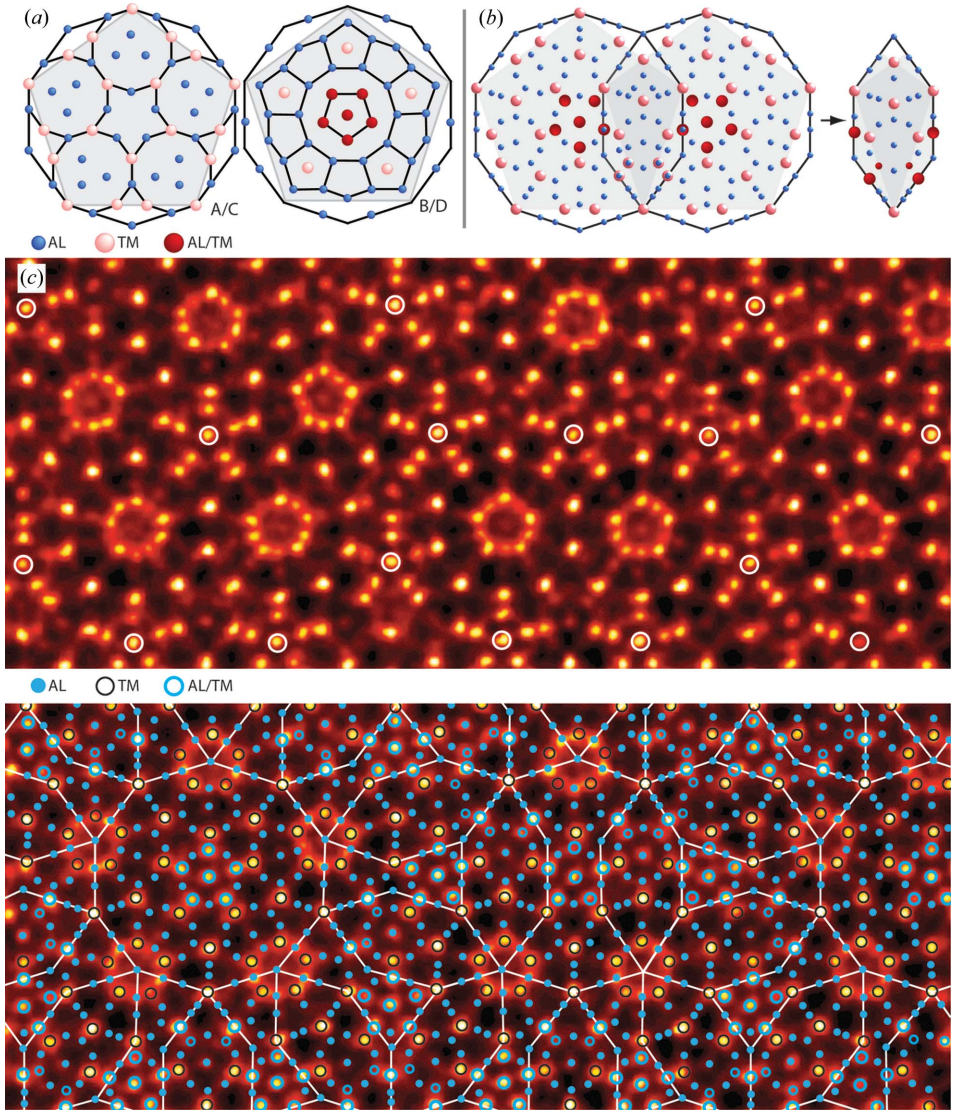

Figure 17
Phase 11 ($Al_{64}Co_{14}Cu_{22}$): (*a*) Atomic decoration of layers *A*/*C* and *B*/*D* projected along the periodic direction. (*b*) Overlap of two clusters. We see the generated flip positions and introduced mixed occupancy within the intersection (*left*) and then an idealized resulting structure of the intersection where all flip positions are eliminated (*right*). (*c*) HAADF-STEM image (Taniguchi & Abe, 2008) of the $Al_{64}Co_{14}Cu_{22}$ phase is shown with and without an overlaid structural model. In the top image, only the cluster centers are marked by white circles. On the image below, the cluster outlines are given in white. This is a high-resolution image that allows the verification of most of the Al sites in the model, additional to the TM sites.

A2. Phase 8, $Al_{73}Fe_{22}Ni_5$

Crystals with nominal composition $Al_{73}Fe_{22}Ni_5$ were synthesized from high-purity elements Al, Fe and Ni (4 N1). A pre-alloy was homogenized and annealed for 264 h at 1163 K, and water-quenched afterwards. Decagonal prismatically shaped crystals of size approximately 50 × 50 × 50 μm^3 were selected for the XRD experiment. The data were collected in-house employing an Oxford single-crystal diffractometer (Onyx CCD detector, graphite monochromator, Mo $K\alpha$ radiation). The 37 628 measured reflections were merged in the Laue group 10/*mmm* to 898 independent reflections with $R_{int} = 0.033$. The experimental resolution was 1.50 Å. The structure solution was performed using the charge-flipping algorithm (Oszlányi & Sütő, 2004; Palatinus, 2004). For further improvement,

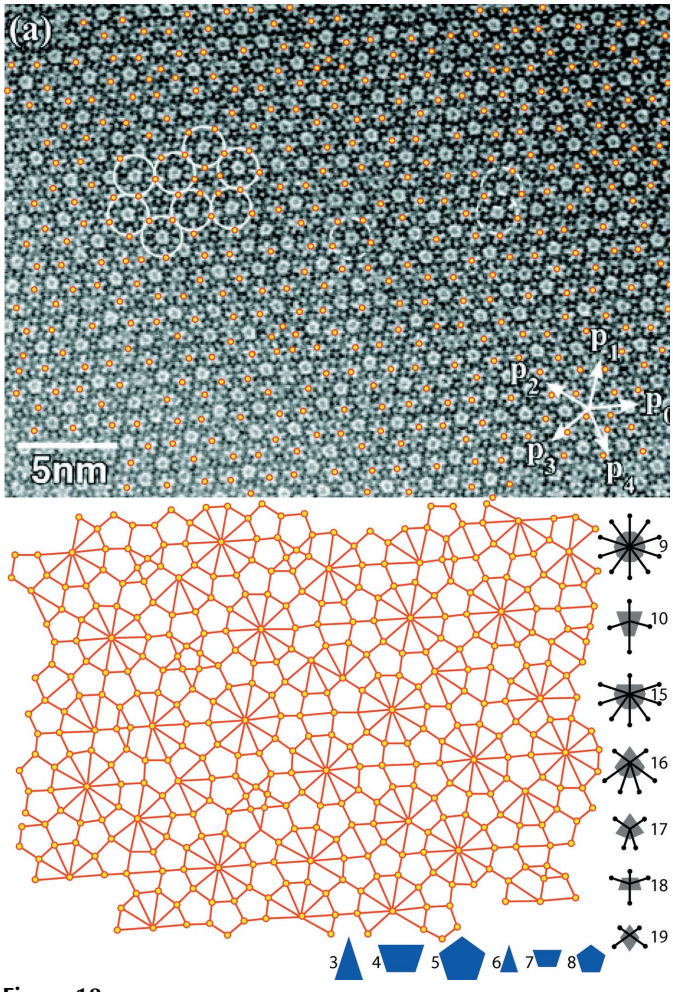

Figure 18
Phase 11 ($Al_{64}Co_{14}Cu_{22}$) HAADF-STEM image (Taniguchi & Abe, 2008) with overlaid tiling vertices corresponding to cluster centers. In the lower part of the figure, we see the extracted tiling (an ideal pentagon tiling of type VT_{13}/DT_5; Masakova *et al.*, 2005), and its Delone (blue) and Voronoi (gray) tiles. It is decorated by positioning the cluster centers on the tiling vertices, where the clusters show only one orientation within the structure.

we used a special averaging approach based on 100 successful charge-flipping structure solutions (Fleischer *et al.*, 2010).

Financial support under grant SNF 200020-121568 is gratefully acknowledged.

References

Abe, E. & Tsai, A.-P. (2004). *J. Non-Cryst. Solids*, **334**, 198–201.
Burkardt, S., Deloudi, S., Erbudak, M., Kortan, A. R., Mungan, M. & Steurer, W. (2008). *J. Phys. Condens. Matter*, **20**, 14006–14016.
Burkardt, S., Erbudak, M. & Mader, R. (2009). *Surf. Sci.* **603**, 867–872.
Deloudi, S., Kobas, M. & Steurer, W. (2006). *Philos. Mag.* **86**, 581–585.
Deloudi, S. & Steurer, W. (2007). *Philos. Mag.* **87**, 2727–2732.
Duguet, T., Unal, B., de Weerd, M., Ledieu, J., Ribeiro, R. A., Canfield, P., Deloudi, S., Steurer, W., Jenks, C., Dubois, J., Fourne, V. & Thiel, P. A. (2009). *Phys. Rev. B*, **80**, 024201.
Fleischer, F. & Steurer, W. (2007). *Philos. Mag.* **87**, 2753–2758.
Fleischer, F., Weber, T., Deloudi, S., Palatinus, L. & Steurer, W. (2010). *J. Appl. Cryst.* **43**, 89–100.
Gummelt, P. (2006). *Z. Kristallogr.* **221**, 582–588.
Henley, C., de Boissieu, M. & Steurer, W. (2006). *Philos. Mag.* **86**, 1131–1151.
Hiraga, K. & Ohsuna, T. (2001). *Mater. Trans. JIM*, **42**, 894–896.
Hiraga, K., Ohsuna, T. & Nishimura, S. (2001). *Mater. Trans. JIM*, **42**, 1081–1084.
Hiraga, K., Ohsuna, T., Sun, W. & Sugiyama, K. (2002). *J. Alloys Compd*, **342**, 110–114.
Mäder, R., Widmer, R., Gröning, P., Deloudi, S., Steurer, W., Heggen, M., Schall, P., Feuerbacher, M. & Gröning, O. (2009). *Phys. Rev. B*, **80**, 035433.
Masakova, Z., Patera, J. & Zich, J. (2005). *J. Phys. A Math. Gen.* **38**, 1947–1960.
Mungan, M., Weisskopf, Y. & Erbudak, M. (2007). *Phys. Rev. B*, **76**, 195443.
Oszlányi, G. & Sütő, A. (2004). *Acta Cryst.* A**60**, 134–141.
Palatinus, L. (2004). *Acta Cryst.* A**60** 604–610.
Saitoh, K., Tsuda, K. & Tanaka, M. (1996). *Philos. Mag. A*, **73**, 387–398.
Saitoh, K., Tsuda, K., Tanaka, M. & Tsai, A. (1999). *Jpn. J. Appl. Phys.* **38**, L671–L674.
Saitoh, K., Yokosawa, T., Tanaka, M. & Tsai, A. P. (1999*a*). *J. Phys. Soc. Jpn*, **68**, 2886–2889.
Saitoh, K., Yokosawa, T., Tanaka, M. & Tsai, A. P. (1999*b*). *J. Electron Microsc.* **48**, 105–114.
Shechtman, D., Blech, I., Gratias, D. & Cahn, J. W. (1984). *Phys. Rev. Lett.* **53**, 1951–1953.
Steurer, W. (2004). *Z. Kristallogr.* **219**, 391–446.
Steurer, W. (2006). *Philos. Mag.* **86**, 1105–1113.
Steurer, W. & Deloudi, S. (2008). *Acta Cryst.* A**64**, 1–11.
Steurer, W., Haibach, T., Zhang, B., Kek, S. & Lück, R. (1993). *Acta Cryst.* B**49**, 661–675.
Steurer, W. & Kuo, K. H. (1990). *Acta Cryst.* B**46**, 703–712.
Sugiyama, K., Nishimura, S. & Hiraga, K. (2002). *J. Alloys Compd*, **342**, 65–71.
Taniguchi, S. & Abe, E. (2008). *Philos. Mag.* **88**, 1949–1958.
Weber, T., Pedersen, B., Gille, P., Frey, F. & Steurer, W. (2008). *Z. Kristallogr.* **223**, 863–867.